





## Quantum chemistry simulation of the electronic properties in $[\text{Au}(\text{NH}_3)_2]\text{NO}_3$ and $[\text{Au}(\text{NCH})_2][\text{AuCl}_4]$ extended unsupported complexes

Fernando Mendizabal, Sebastián Miranda-Rojas & Pablo Castro-Latorre


To cite this article: Fernando Mendizabal, Sebastián Miranda-Rojas & Pablo Castro-Latorre (2020) Quantum chemistry simulation of the electronic properties in  $[\text{Au}(\text{NH}_3)_2]\text{NO}_3$  and  $[\text{Au}(\text{NCH})_2][\text{AuCl}_4]$  extended unsupported complexes, *Molecular Simulation*, 46:7, 521-529, DOI: [10.1080/08927022.2020.1735634](https://doi.org/10.1080/08927022.2020.1735634)


To link to this article: <https://doi.org/10.1080/08927022.2020.1735634>

 View supplementary material 

 Published online: 02 Mar 2020.

 Submit your article to this journal 

 Article views: 36

 View related articles 

 View Crossmark data 



# Quantum chemistry simulation of the electronic properties in $[\text{Au}(\text{NH}_3)_2]\text{NO}_3$ and $[\text{Au}(\text{NCH})_2][\text{AuCl}_4]$ extended unsupported complexes

Fernando Mendizabal<sup>a</sup>, Sebastián Miranda-Rojas<sup>b</sup> and Pablo Castro-Latorre<sup>a</sup>

<sup>a</sup>Departamento de Química, Facultad de Ciencias, Universidad de Chile, Santiago, Chile; <sup>b</sup>Departamento de Ciencias Químicas, Facultad de Ciencias Exactas, Universidad Andres Bello, Santiago, Chile

## ABSTRACT

The understanding of closed-shell interactions has become of tremendous relevance in the ever-growing field of supramolecular chemistry. Here, we present a theoretical study in which we characterised the intermolecular interactions between gold-based building blocks, namely  $([\text{Au}(\text{NH}_3)_2]\text{NO}_3)_n$  ( $n = 1, 2, 4, 8$ ) and  $([\text{Au}(\text{NCH})_2][\text{AuCl}_4])_n$  ( $n = 1, 2$ ). Due to the complex nature of these interactions, several methods were used such as the MP2, CCSD(T), PBE-D3, B3LYP-D3, and CAM-B3LYP-D3 (DFT-D3) levels. In all models were found closed-shell contacts among the gold atoms, interactions that resulted in being consistent with the presence of a high ionic contribution and a dispersion-type interaction. The absorption spectra of these models were calculated by the single excitation time-dependent-DFT (TD-DFT) method and CC2 levels, being the aurophilic interactions mainly responsible for the bands in both types of models. The theoretical models agree with the experimental results.

## ARTICLE HISTORY

Received 5 September 2019  
Accepted 17 February 2020

## KEYWORDS

Aurophilic; dispersion; TD-DFT; post Hartree–Fock; DFT-D3

## 1. Introduction

During the last thirty years, there has been established the existence of gold–gold interactions with  $d^8$  and  $d^{10}$  configurations in intra- and intermolecular complexes [1–3]. This attraction is known as aurophilic interaction [4–7]. Such interaction has been evidenced experimentally by solid state X-ray diffraction [8–12] and Nuclear Magnetic Resonance (NMR) measurements [13,14]. From a theoretical point of view, aurophilic interactions are between 5 and 12 kcal/mol, energetically similar in magnitude to hydrogen bonds [15–19]. This weak metallic contact in complexes and clusters has been understood as the contribution of two terms: dispersion and ionic [3]; while the relativistic effects in the gold–gold interaction contribute approximately 20% to the interaction energy [4]. The dispersion interaction is recovered in the electronic correlation. The theoretical methods most used for describing the aurophilic interaction are post Hartree–Fock (second-order Møller–Plesset perturbation theory (MP2), spin-component-scaled Møller–Plesset perturbation theory (SCS-MP2), Coupled-Cluster Single, Double and Triple (CCSD(T))) and density functional theory (DFT) with dispersion (Grimme approximation) levels [20–24]. In the case of bigger systems, the DFT method is often used.

The closed-shell contacts between the gold atoms after the formation of the complexes are manifested through specific features in their absorption and luminescence properties [15–17]. Such compounds have a behaviour similar to that observed in organic light emitting diodes (OLEDs) [25,26], with a wide range of emission colours. Based on experimental evidence, it has been possible to establish a relationship between emission

energies and the aurophilic distances [27]. This relationship is an essential feature as it allows to understand the structural properties of these complexes through the analysis of the luminescent properties of the materials, which will contribute to the optimisation of materials [15,28,29].

We have focused our attention on two complexes with closed-shell contacts between gold atoms in extended unsupported chains. The first complex is a linear chain with Au(I)–Au(I) ( $d^{10}$ – $d^{10}$ ) as building block in the form of  $[\text{Au}(\text{NH}_3)_2]\text{X}$  ( $\text{X} = \text{Br}, \text{ClO}_4, \text{NO}_3$ ) [30]. The gold(I) cations are arranged in a staggered chain conformation with aurophilic distances between 299.0 and 309.1 pm. The  $[\text{Au}(\text{NH}_3)_2]\text{NO}_3$  complex shows an emission band at 450–600 nm, attributed to gold–gold interactions. Second, the mixed-valent gold complex ( $d^{10}$ – $d^8$ )  $[\text{Au}(\text{NCCy})_2][\text{AuCl}_4]$  (NCCy = cyclohexanecarbonitrile) has been synthesised [31] with a columnar structure of the gold(I/III) rods. The Au(I)–Au(III) ( $d^{10}$ – $d^8$ ) distances are around 332 pm, and the UV/Vis spectrum of this complex in solid state showed a band at 382 nm assigned to gold–gold charge-transfer. There are no reported theoretical studies of these complexes, thereby is still missing a thorough characterisation of the electronic contributions in both complexes.

In this work, we focused on establishing a relationship between aurophilic interactions and excitation spectra in the complexes  $d^{10}$ – $d^{10}$  ( $[\text{Au}(\text{NH}_3)_2]\text{NO}_3$ ) and  $d^{10}$ – $d^8$  ( $[\text{Au}(\text{NCCy})_2][\text{AuCl}_4]$ ). The absorption processes in the complexes will be studied using the approximate Second-Order Coupled Cluster (CC2) and time-dependent density functional theory (TDDFT) calculations.

## 2. Theoretical Models and Calculations

The  $[\text{Au}(\text{NH}_3)_2]\text{NO}_3$  complex in crystal state is modelled using the  $([\text{Au}(\text{NH}_3)_2]\text{NO}_3)_n$  ( $n = 1, 2, 4, 8$ ) systems. They are depicted in Figure 1, where for simplicity; we have omitted the  $\text{NO}_3$  anions in models 3 and 4. These models (2-4) represent the Au(I)-Au(I) ( $d^{10}$ - $d^{10}$ ) aurophilic interaction. The geometries for models 3 and 4 are obtained from model 2, replicating the basic unit of the model 2 at the same distance. On the other hand, the  $[\text{Au}(\text{NCCy})_2][\text{AuCl}_4]$  ( $\text{NCCy} = \text{cyclohexanecarbonitrile}$ ) is represented with models 5 and 6, described in Figure 2. We have replaced the  $-\text{NCCy}$  ligand by  $-\text{NCH}$  to reduce the computing time.

The geometries are fully optimised at the scalar relativistic MP2, CCSD(T), PBE (Perdew-Burke-Ernzerhof) [32], B3LYP (Becke, 3-parameter, Lee-Yang-Parr) [33], and CAM-B3LYP (Coulomb Attenuated Method - Becke, 3-parameter, Lee-Yang-Parr) [34] levels for each fragment in the models. Grimme's dispersion correction is used to incorporate a proper description of the weak interactions when using those functionals, in what is nowadays known as the DFT-D3 level with Becke-Johnson (BJ) correction [35]. The gold-gold interaction energy ( $\Delta E_{\text{int}}$ ) and geometric equilibrium ( $R_e$ ) of the complexes are obtained with a counterpoise correction for the basis-set superposition error (BSSE) [36].

Single point calculations of the equilibrium geometries were used to study the excitation spectra by PBE, B3LYP, and CAM-B3LYP (DFT). The excitation energy was obtained using the time-dependent perturbation theory approach (TD) [37]. Moreover, excitation energies and oscillator strengths are calculated at the approximate second-order coupled cluster (CC2) level using the scaled opposite-spin (SOS) approximation [38]. Also, we have used the Spin-Component-Scaled (SCS)-CC2 method [39]. SOS-CC2 and SCS-CC2 attenuate the overestimation given by the MP2 method. We have used the equilibrium distance ( $R_e$ ) estimated at the MP2 level to calculate the excitation spectrum at CC2. This method consists

involves the Laplace transformation (LT) algorithm and the reduced-virtual-space (RVS) approximation. The RVS cut-off threshold was 60 eV [38]. The results obtained using the CC2 and SOS-CC2 correlated methods are compared with those calculated at the time-dependent density functional theory (TDDFT) level using a couple of functionals. TDDFT is widely used in excited state studies of large molecules, because of its good performance and its relatively low computational costs. However, since TDDFT calculations might suffer from charge transfer problems, the reliability of the obtained results should be assessed by comparing with the results calculated at higher levels of theory [39].

The calculations were carried out using the Turbomole 7.3 [40], and Gaussian09 [41] programme packages. The 19 valence-electrons (VE) of Au quasi-relativistic (QR) pseudo-potential (PP) of Andrae [42] were employed. We used two  $f$ -type polarisation functions on gold ( $\alpha_f = 0.20, 1.19$ ). Also, the C, N, O, and Cl atoms were treated through PPs, using double-zeta basis sets with the addition of one  $d$ -type polarisation function [43]. For the H atom, a double-zeta basis set plus one  $p$ -type polarisation function was used [44].

## 3. Results and Discussion

### 3.1. Aurophilic Attractions

Some selected geometric parameters of the fully optimised monomers are summarised in Table 1. Meanwhile, the gold-gold interaction energies and equilibrium distances for models 2, 5, and 6 are listed in Table 2. The gold-gold distances are overestimated for all models, although the experimental trend is maintained. This result is within expectations since it has been shown that the CCSD(T) method described a proper estimation of the aurophilic interaction [45]. The electronic correlation effects play an essential role in the stability of these type of systems, and therefore, it will affect the equilibrium distances and the interaction

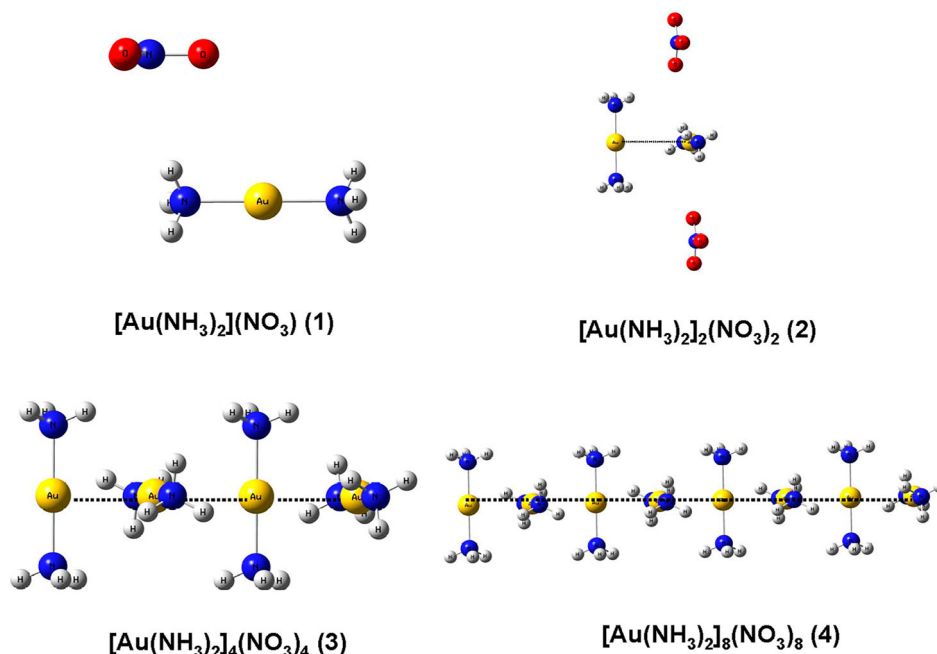
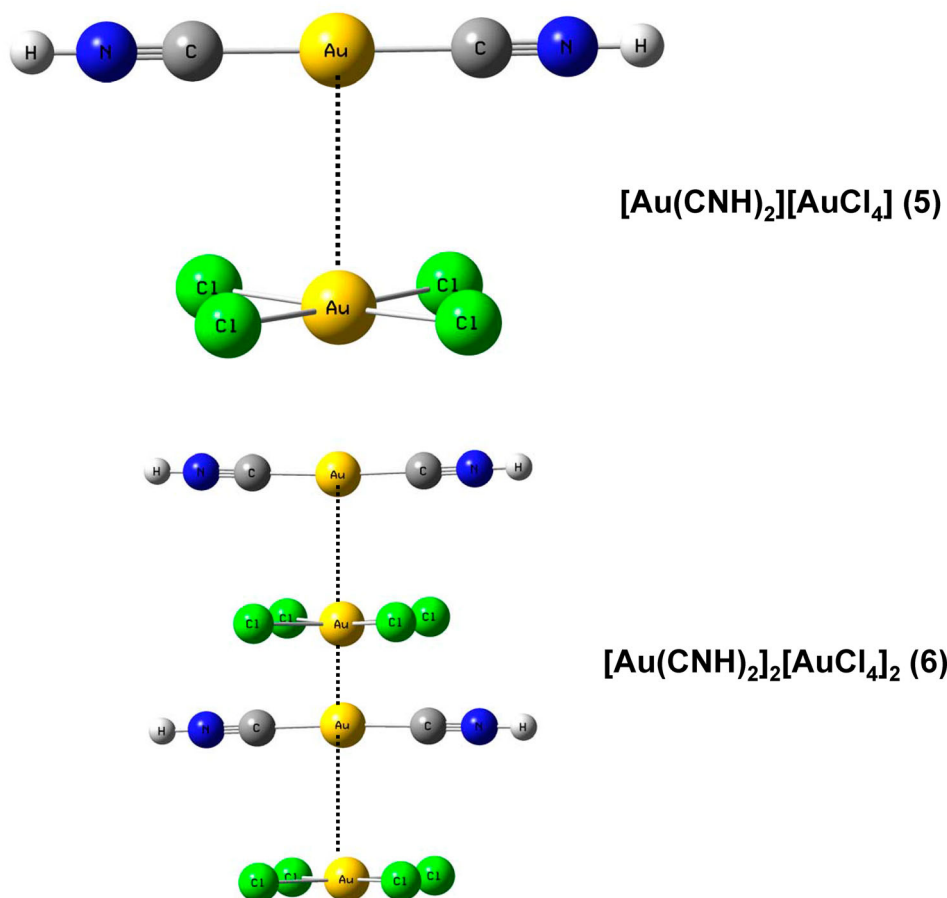


Figure 1. Theoretical  $[\text{Au}(\text{NH}_3)_2]_n(\text{NO}_3)_n$  models ( $n = 1, 2, 4, 8$ ) 1-4.



**Figure 2.** Theoretical  $[\text{Au}(\text{NCH})_2][\text{AuCl}_4]$  (5) and  $([\text{Au}(\text{NCH})_2][\text{AuCl}_4])_2$  models (6).

energies. To estimate the contribution of the electronic correlation effect ( $\Delta E(\text{corr})$ ) in the intermolecular gold–gold distances, we compared each model at the Hartree–Fock (HF) and MP2 levels ( $\Delta E(\text{MP2-HF})$ ); HF and CCSD(T) levels ( $\Delta E(\text{CCSD(T)-HF})$ ); DFT and DFT-D3 ( $\Delta E(\text{DFT-D3})-(\text{DFT})$ ).

The obtained tendencies are shown in Table 2. According to this, we found that for model 2, the electronic correlation effect is in the magnitude range of dispersion-type van der Waals interactions. At the HF level, there is a component due to the

charge of the model. The DFT results are within the same range as MP2. Moreover, at the CCSD(T) level shows a lower magnitude as is expected, within the estimates with other systems reported in the literature [45]. Based on these results,

**Table 2.** Optimised Au–Au distance,  $R_e$ , for the models at the HF, MP2 and DFT-D3 levels. Equilibrium distance  $R_e$  in pm; interaction energy  $\Delta E_{\text{int}}$  in kcal/mol.

Model	Method	$R_e$	$\Delta E_{\text{int}}$	$\Delta E(\text{corr})^a$
$[\text{Au}(\text{NH}_3)_2] - [\text{Au}(\text{NH}_3)_2](\text{NO}_3)_2$ (2)	HF	339.8	−9.24	
	MP2	289.5	−24.35	−19.28
	CCSD(T)	299.1	−20.61	−13.75
	PBE-D3	299.3	−30.12	−24.12
	B3LYP-D3	303.5	−28.78	−22.28
$[\text{Au}(\text{NCH})_2] - [\text{AuCl}_4]$ (5)	CAM-B3LYP-D3	310.4	−22.65	−19.43
	HF	342.6	−47.38	
	MP2	306.9	−69.75	−25.64
	CCSD(T)	321.1	−61.75	−15.41
	PBE-D3	303.8	−80.90	−25.98
$[\text{Au}(\text{NCH})_2][\text{AuCl}_4] - [\text{Au}(\text{NCH})_2][\text{AuCl}_4]$ (6)	B3LYP-D3	312.3	−82.21	−22.83
	CAM-B3LYP-D3	307.6	−81.41	−24.45
	HF	332.1	1.22	
	MP2	332.1	−10.29	−11.51
	CCSD(T)	347.6	−7.88	−8.53
$[\text{Au}(\text{NCH})_2]^{-2}$	PBE-D3	337.6	−9.68	−6.60
	B3LYP-D3	340.9	−11.92	−11.42
	CAM-B3LYP-D3	332.1	−10.60	−10.03
	Exp. [30]	341.4		
	Exp. [30]	309.1		
$[\text{Au}(\text{NCCy})_2][\text{AuCl}_4]$	Exp. [31]	325.0		

**Table 1.** Main geometric parameters of the monomers used. Distances are in pm.

Monomer	Method	Au–N	Au–Cl	N–H	C–N	N–H
$[\text{Au}(\text{NH}_3)_2](\text{NO}_3)$	MP2	201.1		102.6		
	CCSD(T)	204.2		102.7		
	PBE-D3	204.2		104.2		
	B3LYP-D3	206.7		102.5		
	CAM-B3LYP-D3	205.3		102.4		
	Exp. [34]	204.0				
$[\text{Au}(\text{NCH})_2]^+$	MP2	195.9			116.3	101.0
	CCSD(T)	200.2			116.2	101.6
	PBE-D3	196.6			116.1	101.5
	B3LYP-D3	198.7			114.9	100.9
	CAM-B3LYP-D3	199.5			114.8	100.9
	Exp. <sup>a</sup> [35]	195.6			113.9	
$[\text{AuCl}_4]^{-2}$	MP2		230.3			
	CCSD(T)		233.0			
	PBE-D3		233.6			
	B3LYP-D3		234.2			
	CAM-B3LYP-D3		232.3			
	Exp. <sup>a</sup> [35]		227.0			

<sup>a</sup> $[\text{Au}(\text{NCCy})_2][\text{AuCl}_4]$  experimental X-ray.

<sup>a</sup> $\Delta E(\text{MP2-HF})$ ;  $\Delta E((\text{DFT-D3})-\text{DFT})$  approximate D3 in DFT level.

we have used the geometry of the model **2** to build models **3** ( $[\text{Au}(\text{NH}_3)_2]_4$ ) and **4** ( $[\text{Au}(\text{NH}_3)_2]_8$ ).

When we use simplified models such as **5** and **6** to describe the interaction between gold(I) and gold(III), the interaction energies are increased to magnitudes associated with an ionic character. The calculations can reproduce the structural trends found in the experimental data. Thus, the interaction energy at the MP2 level in model **5** is composed of 73% of ionic term and 27% of electronic correlation. It is assumed that the ionic interactions are responsible for the attractive behaviour obtained at the HF level. The additional stabilisation achieved at the MP2 level is due to the introduction of dispersion-type correlation effects and charge transfer contributions. At the CCSD(T), the gold–gold distance is larger and the interaction energy is lower than the obtained at the MP2 level. The electronic correlation in CCSD(T) is lower. At the DFT level, the ionic interaction is 82% and the correlation effect is 18%. The magnitudes of the Au(I)–Au(III) interactions are in the range of other complexes studied in the literature, such as in  $[\text{ClAu}(\text{I})\text{PH}_3][\text{Cl}_3\text{Au}(\text{III})\text{PH}_3]$  [46].

Moreover, we have built one linear tetramer unit defined as model **6** depicted in Figure 2, and the calculated interaction distances and energies are summarised in Table 2. Due to the relevance of the dispersive term in the interaction between the subunits, as expected at HF level, we found no energy minimum. It is because both fragments are neutrally charged. Model **6** shows a classic aurophilic interaction between the gold atoms inferred from the energy difference of 11.5 kcal/mol between HF and MP2. Similar results were obtained from the DFT–D3 level of theory. The CCSD(T) result shows a decrease in the interaction energy in 7.8 kcal/mol, 23% less respect the same result at the MP2 level. In all levels, the gold–gold distances are found to be longer than the experimental results. At the HF level is repulsive. The results of the model **6** show a classic aurophilic contact [45].

The charge of the gold atoms in models **2**, **5**, and **6** have been obtained using the NBO method [47]. From this, it is possible to identify the ionic effects contributing to the gold–gold interactions in the different models (see Table A1 in supplementary material). The data for all the models showed a reduction of the formal oxidation state of gold(I) and gold(III). The smallest charge is found on gold(I) in the calculated models, whereas a more substantial positive charge is concentrated on the gold (III), as expected. However, in all the models, we found the same magnitude of the charge of the gold atoms, which would give rise to a repulsive interaction.

### 3.2. Excitation energy calculations

The UV–Vis spectra have been calculated at the TDDFT level using the PBE, B3LYP and CAM–B3LYP functionals. Also, the excitation energies of the models were analysed at the SOS–CC2 level. We calculated the allowed spin singlet transition for these systems, based on the ground state structures of models **1–6**. The goal was to evaluate the electronic structure of the excited state by direct electronic excitations. The allowed transitions for models **1–4** are listed in Table 3, while for models **5** and **6** are presented in Table 4.

Similar excitation energies are obtained for models **1–4** at the DFT and SOS–CC2 levels. However, in all models, the

**Table 3.** The strongest singlet excitation energies calculated for models **1–4** are compared to experimental data [34]. The excitation energies and oscillator strengths have been calculated at the TDDFT and CC2 levels. The orbital contributions and the character of the transitions are also given.

Model	Method	$\lambda_{\text{calc}}/\text{nm}$	$f^a$	Contribution <sup>b</sup>	Transition type
$[\text{Au}(\text{NH}_3)_2](\text{NO}_3)$ (1)	PBE	175	0.1093	29a → 32a (80)	MMCT ( $\text{dz}^2 \rightarrow \text{p}$ )
	B3LYP	175	0.1093	29a → 32a (89)	MMCT ( $\text{dz}^2 \rightarrow \text{p}$ )
	CAM-B3LYP	175	0.0990	29a → 32a (85)	MMCT ( $\text{dz}^2 \rightarrow \text{p}$ )
	SOS-CC2	172	0.1575	29a → 32a (73)	MMCT ( $\text{dz}^2 \rightarrow \text{p}$ )
$[\text{Au}(\text{NH}_3)_2]_2(\text{NO}_3)_2$ (2)	PBE	205	0.3496	58a → 63a (76)	MMCT ( $\text{dz}^2 + \text{dx}^2 - \text{y}^{2*} \rightarrow \text{pz}$ )
	B3LYP	195	0.3048	58a → 63a (60)	MMCT ( $\text{dz}^2 + \text{dx}^2 - \text{y}^{2*} \rightarrow \text{pz}$ )
	CAM-B3LYP	190	0.4470	58a → 63a (85)	MMCT ( $\text{dz}^2 + \text{dx}^2 - \text{y}^{2*} \rightarrow \text{pz}$ )
	SOS-CC2	191	0.6522	58a → 63a (70)	MMCT ( $\text{dz}^2 + \text{dx}^2 - \text{y}^{2*} \rightarrow \text{pz}$ )
$[\text{Au}(\text{NH}_3)_2]_4(\text{NO}_3)_4$ (3)	PBE	284	0.5632	116a → 121a (85)	MMCT ( $\text{dz}^2 + \text{dx}^2 - \text{y}^{2*} \rightarrow \text{pz} + \text{dz}^2$ )
		249	0.2672	115a → 120a (85)	MMCT ( $\text{dz}^2 + \text{dx}^2 - \text{y}^{2*} \rightarrow \text{s} + \text{pz}$ )
		230	0.2551	116a → 125a (85)	MMCT ( $\text{dz}^2 + \text{dx}^2 - \text{y}^{2*} \rightarrow \text{pz}$ )
	B3LYP	251	0.9864	116a → 121a (97)	MMCT ( $\text{dz}^2 + \text{dx}^2 - \text{y}^{2*} \rightarrow \text{pz} + \text{dz}^2$ )
		204	0.1984	116a → 125a (58)	MMCT ( $\text{dz}^2 + \text{dx}^2 - \text{y}^{2*} \rightarrow \text{s} + \text{pz}$ )
	CAM-B3LYP	236	1.2165	116a → 120a (86)	MMCT ( $\text{dz}^2 + \text{dx}^2 - \text{y}^{2*} \rightarrow \text{pz} + \text{dz}^2$ )
		189	0.2290	116a → 125a (52)	MMCT ( $\text{dz}^2 + \text{dx}^2 - \text{y}^{2*} \rightarrow \text{s} + \text{pz}$ )
	SOS-CC2	241	1.5750	116a → 121a (81)	MMCT ( $\text{dz}^2 + \text{dx}^2 - \text{y}^{2*} \rightarrow \text{pz} + \text{dz}^2$ )
		187	0.1685	116a → 124a (44)	MMCT ( $\text{dz}^2 + \text{dx}^2 - \text{y}^{2*} \rightarrow \text{s} + \text{pz}$ )
	$[\text{Au}(\text{NH}_3)_2]_8(\text{NO}_3)_8$ (4)	PBE	481	0.3155	232a → 235a (78)
		375	0.5875	231a → 239a (63)	MMCT ( $\text{dz}^2 + \text{dx}^2 - \text{y}^{2*} \rightarrow \text{s} + \text{pz}$ )
		357	0.1286	230a → 226a (93)	MMCT ( $\text{dz}^2 + \text{dx}^2 - \text{y}^{2*} \rightarrow \text{pz} + \text{dz}^2$ )
B3LYP		365	0.4993	232a → 237a (69)	MMCT ( $\text{dz}^2 + \text{dx}^2 - \text{y}^{2*} \rightarrow \text{pz} + \text{dz}^2$ )
		317	0.6873	232a → 238a (64)	MMCT ( $\text{dz}^2 + \text{dx}^2 - \text{y}^{2*} \rightarrow \text{s} + \text{pz}$ )
		269	0.6547	230a → 237a (81)	MMCT ( $\text{dz}^2 + \text{dx}^2 - \text{y}^{2*} \rightarrow \text{pz} + \text{dz}^2$ )
CAM-B3LYP		290	0.6445	232a → 233a (65)	MMCT ( $\text{dz}^2 + \text{dx}^2 - \text{y}^{2*} \rightarrow \text{pz} + \text{dz}^2$ )
		287	1.9254	232a → 236a (60)	MMCT ( $\text{dz}^2 + \text{dx}^2 - \text{y}^{2*} \rightarrow \text{s} + \text{pz}$ )
		228	0.5269	232a → 245a (63)	MMCT ( $\text{dz}^2 + \text{dx}^2 - \text{y}^{2*} \rightarrow \text{pz} + \text{dz}^2$ )
SOS-CC2		311	0.2643	232a → 233a (49)	MMCT ( $\text{dz}^2 + \text{dx}^2 - \text{y}^{2*} \rightarrow \text{pz} + \text{dz}^2$ )
		305	2.5870	232a → 237a (51)	MMCT ( $\text{dz}^2 + \text{dx}^2 - \text{y}^{2*} \rightarrow \text{s} + \text{pz}$ )
		277	0.3406	232a → 245a (36)	MMCT ( $\text{dz}^2 + \text{dx}^2 - \text{y}^{2*} \rightarrow \text{pz} + \text{dz}^2$ )
$[\text{Au}(\text{NH}_3)_2](\text{NO}_3)$		Solid [30]	450–650		

<sup>a</sup>Oscillator strength.

<sup>b</sup>Values are  $|\text{coeff.}|^2 \times 100$ .

band transitions calculated at the DFT levels were red shifted as compared to the SOS–CC2 value. If we analyse the first transition in the model **4**, we found that with PBE level it appears at 481 nm, at 365 nm with B3LYP, at 290 nm with CAM–B3LYP and at 311 nm with SOS–CC2. Moreover, we have performed SCS–CC2 calculations. The results are summarised in Table



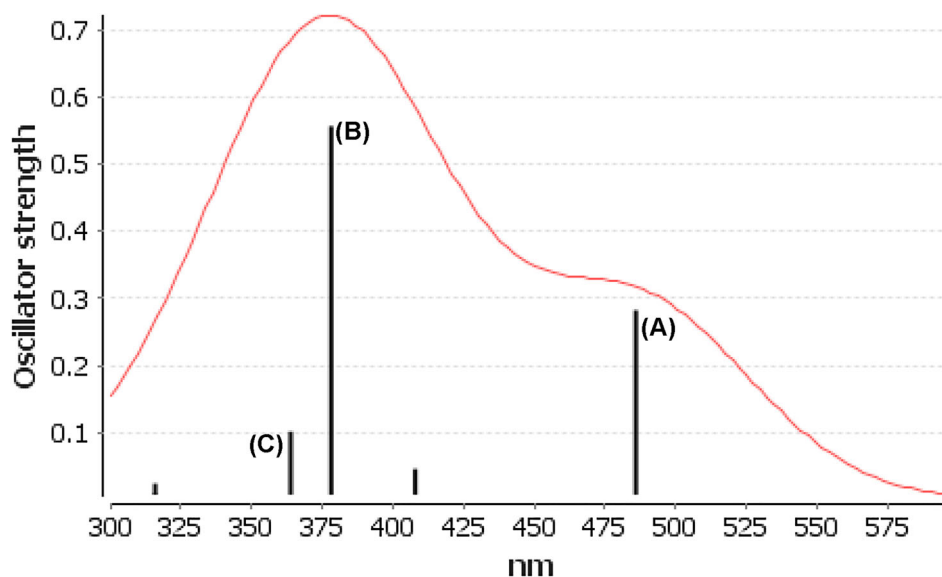
**Table 4.** The strongest singlet excitation energies calculated for models **5** and **6** are compared to experimental data [31]. The excitation energies and oscillator strengths have been calculated at the TD-DFT and CC2 levels. The orbital contributions and the character of the transitions are also given.

Model	Method	$\lambda_{\text{calc}}/\text{nm}$	$f^a$	Contribution <sup>b</sup>	Transition type	
[Au(NCH) <sub>2</sub> ][AuCl <sub>4</sub> ] ( <b>5</b> )	PBE	400	0.0081	41a → 46a (99)	MLMLCT (dxz + pz* → π)	
		321	0.1218	36a → 45a (92)	MLMLCT (dx <sup>2</sup> -y <sup>2</sup> * → π)	
		243	0.1420	33a → 44a (42)	MLMLCT (π* → π)	
	B3LYP	414	0.0118	39a → 44a (95)	MLMLCT (dxz + pz* → π)	
		261	0.1831	36a → 45a (96)	MLMLCT (dx <sup>2</sup> -y <sup>2</sup> * → π)	
		240	0.2707	33a → 44a (71)	MLMLCT (π* → π)	
	CAM-B3LYP	313	0.0265	40a → 46a (90)	MLMLCT (dxz + pz* → π)	
		244	0.2562	36a → 45a (80)	MLMLCT (dx <sup>2</sup> -y <sup>2</sup> * → π)	
		206	0.2787	33a → 46a (78)	MIMLCT (π* → π)	
	SOS-CC2	340	0.0374	42a → 44a (82)	MLMLCT (dxz + pz* → π)	
		234	0.3446	40a → 45a (44)	MLMLCT (dx <sup>2</sup> -y <sup>2</sup> * → π)	
		216	0.2090	33a → 44a (33)	MLMLCT (π* → π)	
	[Au(NCH) <sub>2</sub> ] <sub>2</sub> [AuCl <sub>4</sub> ] <sub>2</sub> ( <b>6</b> )	PBE	492	0.0537	81a → 89a (98)	LMLCT (π → s + pz + π)
			328	0.3591	81a → 91a (91)	LMLCT (π → pz + π)
314			0.0885	70a → 89a (79)	MLML (dz <sup>2</sup> + π → s + pz + π)	
253			0.0900	69a → 88a (30)	MLML (dz <sup>2</sup> + π → pz + π)	
B3LYP		413	0.0122	82a → 88a (95)	LMLCT (π → s + pz + π)	
		265	0.4730	80a → 91a (83)	LMLCT (π → pz + π)	
		238	0.3074	68a → 88a (59)	MLML (dz <sup>2</sup> + π → pz + π)	
CAM-B3LYP		302	0.0144	75a → 87a (89)	LMLCT (π → pz + π)	
		301	0.0384	82a → 90a (89)	MLML (dz <sup>2</sup> + π → s + pz + π)	
		240	0.6587	78a → 92a (53)	MLML (dz <sup>2</sup> + π → pz + π)	
SOS-CC2		402	0.0077	74a → 87a (56)	LMLCT (π → pz + π)	
		348	0.0237	75a → 87a (65)	LMLCT (π → pz + π)	
		235	0.3547	81a → 91a (91)	MLML (dz <sup>2</sup> + π → pz + π)	
[Au(NCCy) <sub>2</sub> ][AuCl <sub>4</sub> ]		Solid [31] <sup>c</sup>	331, 248 <sup>c</sup>			

<sup>a</sup>Oscillator strength.<sup>b</sup>Values are |coeff.<sup>2</sup> × 100.<sup>c</sup>ATR-UV/Vis solid spectrum. 331 and 248 nm are maximum peaks 382, 432, and 462 nm are shoulder bands.

A2 of the supplementary material. It is obtained a blue shift of the electronic transitions. The comparison of the excitation energies and oscillator strengths calculated at the four levels of theory show that the excitation energies calculated at the PBE level are generally smaller than those obtained with the B3LYP, CAM-B3LYP and SOS-CC2 calculations. More states are also obtained at the PBE level suggesting that there are charge transfer problems in the high-energy region of the visible part of the absorption spectra. Very similar absorption spectra were obtained at the B3LYP, CAM-B3LYP and SOS-CC2 levels in the studied energy range.

For [Au(NCH)<sub>2</sub>][AuCl<sub>4</sub>] (**5**) and ([Au(NCH)<sub>2</sub>][AuCl<sub>4</sub>])<sub>2</sub> (**6**), the band calculated at the PBE level is red shifted relative to the value obtained using B3LYP, CAM-B3LYP, and SOS-CC2 (see Table 4). The same holds for the other studied excitation energies. Similar oscillator strengths were obtained at the four levels of theory. The SCS-CC2 results in both models show bands at higher energy (shorter wavelength). These data are shown in Table A3 of the supplementary material. The transition wavelengths of the strong transitions calculated at the PBE level are in better agreement with the experimental values than those obtained at the other computational levels.

**Figure 3.** Electronic spectra at the PBE level calculated for [Au(NH<sub>3</sub>)<sub>2</sub>]<sub>8</sub>(NO<sub>3</sub>)<sub>8</sub> (**4**).

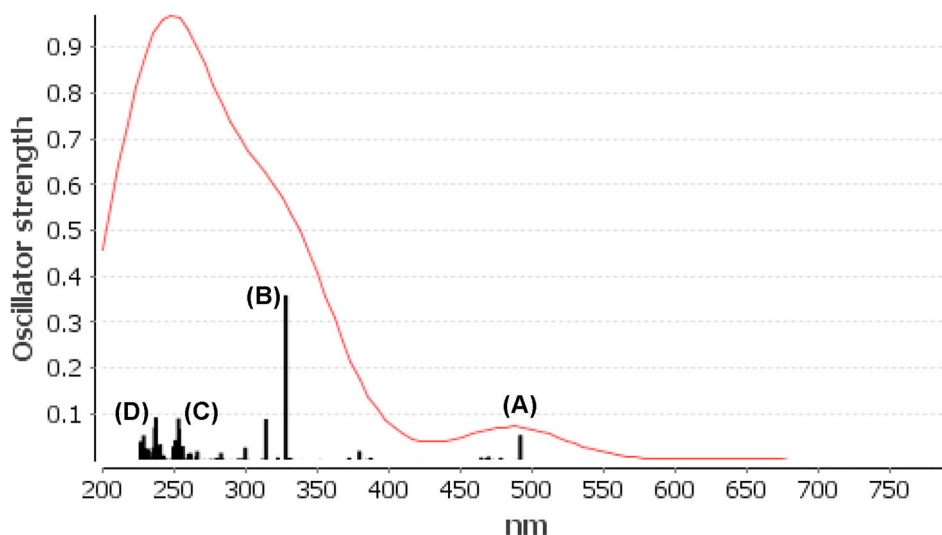


**Figure 4.** Electronic spectra at the PBE level calculated for  $([\text{Au}(\text{NCH}_2)_2][\text{AuCl}_4])_2$  (**6**).

All the methods used in this work show the same qualitative trend. It is possible to observe that the electronic transitions are red shifted when the increases in the size of the models. The results obtained with the PBE method are closer to the experimental data. Thus, we used the main transitions obtained with PBE method, and the compares with the excitation energies calculated by the other methods used in this work. We discuss only the properties of the  $[\text{Au}(\text{NH}_3)_2]_8(\text{NO}_3)_8$  (**4**) and  $([\text{Au}(\text{NCH}_2)_2][\text{AuCl}_4])_2$  (**6**) models at the PBE levels. The results are shown in Figures 3 and 4, respectively. Moreover, the electronic transitions are summarised in Figure 5 for  $[\text{Au}(\text{NH}_3)_2]_8(\text{NO}_3)_8$  and in Figure 6 for  $([\text{Au}(\text{NCH}_2)_2][\text{AuCl}_4])_2$ . Electronic transitions and the active molecular orbitals in the SOS-CC2 calculation has been described in Figure A1 in the

supplementary material for the  $[\text{Au}(\text{NH}_3)_2]_n(\text{NO}_3)_n$  ( $n = 1, 2, 4, 8$ ) models (1-4). These results are qualitatively same that the obtained by the PBE method (in Figures 5 and A2).

### 3.2.1. $[\text{Au}(\text{NH}_3)_2]_8(\text{NO}_3)_8$

This gold complex shows an experimental spectrum with a band between 450 and 650 nm [30]. We increase the size of the models from one to eight units, regardless of the method used; we can see a shift of the theoretical absorption bands. So they are approaching the experimental spectrum. We do aim to highlight the trend that is obtained follows the experimental absorption band associated with gold-gold interaction.

The calculated spectra show a major transition that changes depending on the method used. They are shown in Table 3.

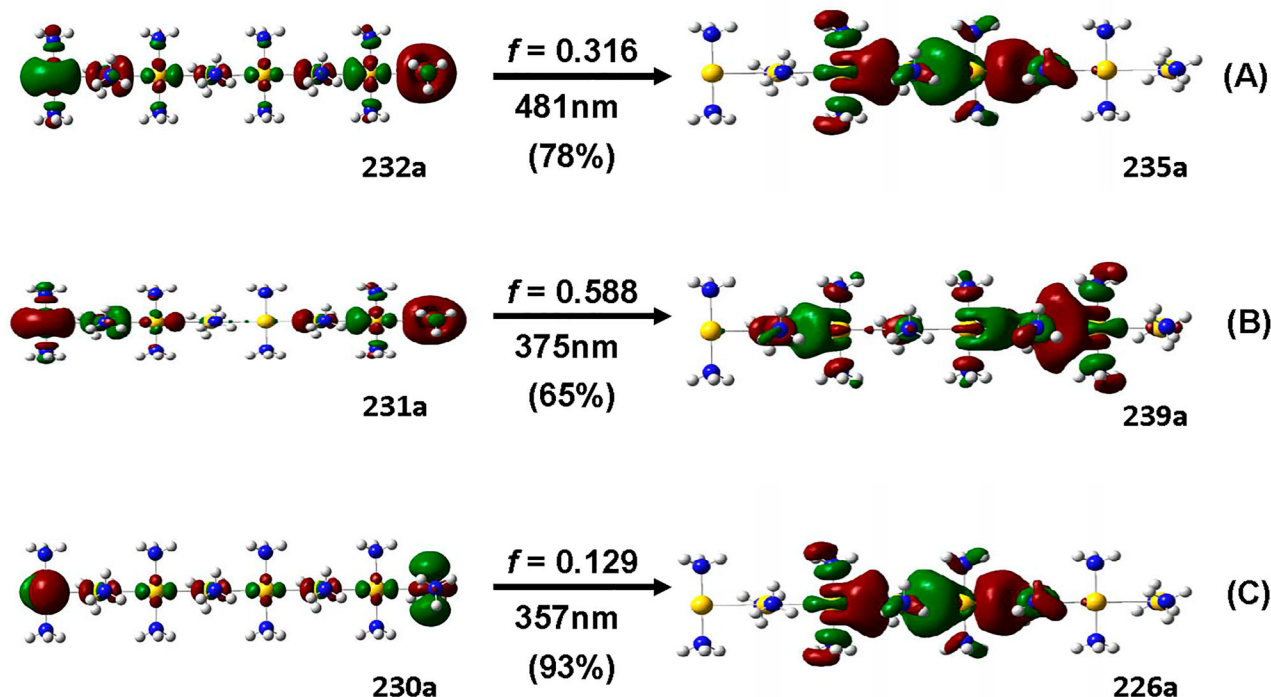


**Figure 5.** Most important active molecular orbitals in the electronic transitions of the  $[\text{Au}(\text{NH}_3)_2]_8(\text{NO}_3)_8$  (**4**) model at the PBE level.

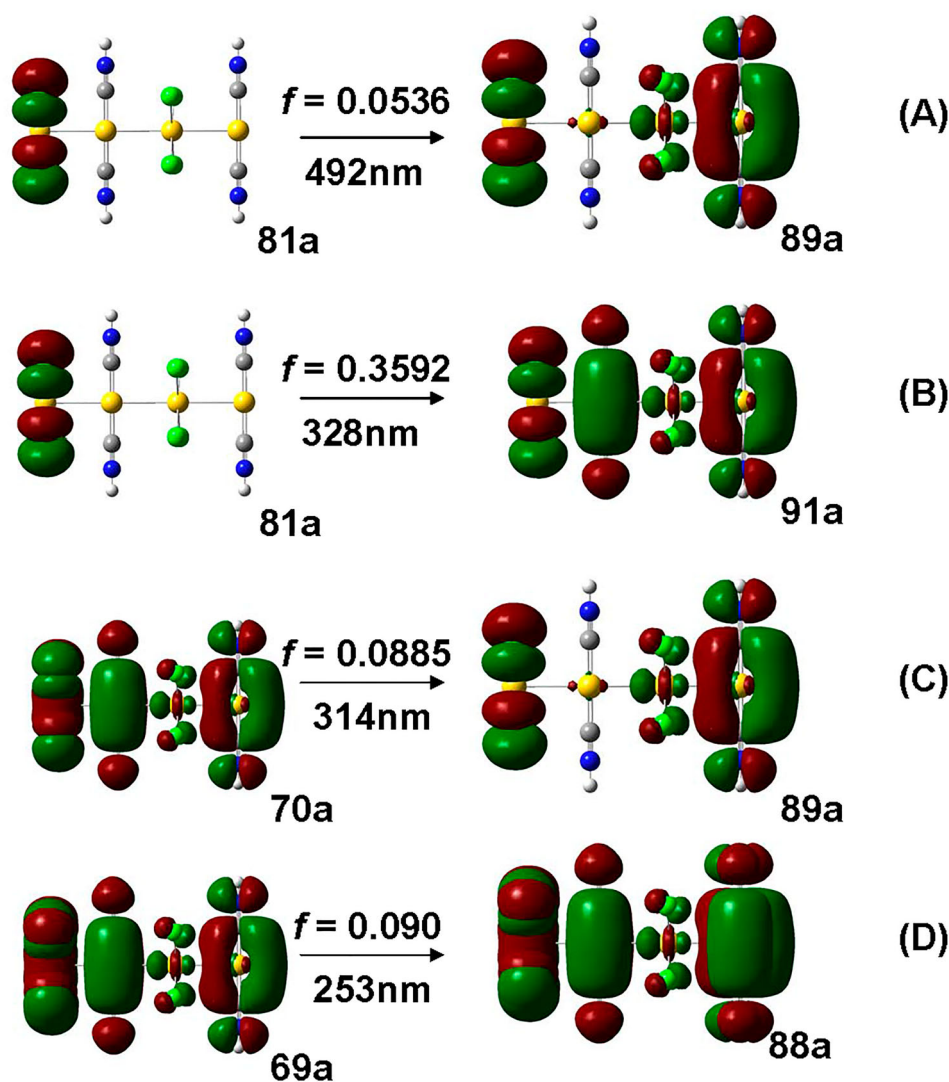


**Figure 6.** Most important active molecular orbitals in the electronic transitions of the  $([\text{Au}(\text{NCH})_2][\text{AuCl}_4])_2$  (**6**) model at the PBE level.

The complexes show oligomeric structures, so an agreement is at the semiquantitative level. The  $[\text{Au}(\text{NH}_3)_2]_8(\text{NO}_3)_8$  model has three important transitions at 481 nm (A), 375 nm (B), and 357 nm (C). They are caused mainly by metal–metal charge transfer (MMCT), mostly centred among the gold atoms.

### 3.2.2. $[\text{Au}(\text{NCH})_2]_2[\text{AuCl}_4]_2$

The theoretical transitions of the models (**5** and **6**) and experimental spectroscopic absorption data are summarised in Table 4. The experimental spectra depicted by the solid line show two intense absorption bands at 331, and 248 nm [31]. Besides, three shoulders at 382, 432, and 462 nm are identified. According to the data presented in Table 4, the largest model (**6**) was able to reproduce the experimental spectrum, also highlighting the good performance of PBE and CC2 methodologies (see Figure 4).

The spectrum calculated for model **6** at the PBE level shows theoretical transitions at 492 nm (A), 328 nm (B), 314 nm (C), and 253 nm (D). The transitions are assigned to  $81a \rightarrow 91a$  (328 nm) and  $69a \rightarrow 88a$  (253 nm), in agreement with the experimental bands (331 and 248 nm). These bands correspond to a ligand-to-metal–ligand charge transfer

(LMLCT) and metal–ligand-to-metal–ligand charge transfer (MLMLCT).

### 3.3. Auophilic Distance and Excitation Energies

The auophilic interactions are considered in most complexes to be responsible for the electronic spectroscopic features, that are highly dependent on the gold–gold distance [48]. In the last time, some compounds with auophilic contacts under the action of pressure or concentration, e.g.  $[\text{Au}(\text{C}_6\text{Cl}_5)_2]$ ,  $\text{Ag}([9]\text{aneS}_3)_2$  [27] and  $\text{K}[\text{Au}(\text{CN})_2]$  [49], have shown that the absorption and emission bands change with the reduction or lengthening of the gold–gold distance.

In this section, we have used  $[\text{Au}(\text{NH}_3)_2]_n(\text{NO}_3)_n$  ( $n = 2, 4$ ) (**2, 3**) models to characterise the relationship between the gold–gold distance and the absorption band associated to the auophilic interaction. For this purpose, we calculated the electronic transitions at increasing gold–gold distance starting from the equilibrium geometry. The results are summarised in Table 5 for the  $[\text{Au}(\text{NH}_3)_2]_2(\text{NO}_3)_2$  model (**2**) and in Table A4 for the  $[\text{Au}(\text{NH}_3)_2]_4(\text{NO}_3)_4$  model (**4**). These are



**Table 5.** The strong singlet excitation energy calculated for  $[\text{Au}(\text{NH}_3)_2]_2(\text{NO}_3)_2$  (**2**) at different Au—Au (pm) distances, correlating wavelength ( $\lambda$ ) and oscillator strength ( $f$ ).

Au—Au	PBE		SOS-CC2		SCS-CC2	
	$\lambda$	$f$	$\lambda$	$f$	$\lambda$	$f$
$R_e$	205	0.350	191	0.652	187	0.629
340	197	0.304	178	0.530	176	0.510
380	196	0.133	174	0.351	171	0.347
420	191	0.121	173	0.308	170	0.319
500	190	0.100	172	0.293	169	0.310
1000	189	0.006	170	0.010	169	0.016

$R_e$ : equilibrium distance Au—Au in model 2 at the PBE, CC2 (MP2) and SCS-CC2 (SCS-MP2) levels.

calculated at the PBE, SOS-CC2 and SCS-CC2 levels. Regardless of the method used, with the increase of the gold–gold distance is possible to appreciate how the absorption band associated with the aurophilic interaction is blue-shifted towards a shorter wavelength (higher energy). It is in accordance with the previous results shown in section 3.2 and is complemented by the equilibrium models of section 3.1. Although the aurophilic interaction is not relevant to estimate the electronic properties, it is mainly the equilibrium distance in the first electronic state with which these optical properties are estimated.

#### 4. Conclusion

Theoretical calculations at the MP2, CCSD(T) and DFT-D3 levels were suitable to describe the aurophilic interaction present in the proposed models with configurations  $d^{10}$ - $d^{10}$  and  $d^{10}$ - $d^8$ . Through TDDFT/PBE calculations, we were able to reproduce the experimental excitation spectra and rationalise the relationship between the gold–gold distance and the shift in the main absorption bands. For all models, there is a strong dependence between the gold–gold intermolecular contact and the absorption bands, with a red shift effect that is observed in the experimental complexes in the solid state. Finally, our results showed that the aurophilic attraction is mainly responsible for the MMCT in  $[\text{Au}(\text{NH}_3)_2]_n(\text{NO}_3)_n$  models ( $n = 2, 4, 8$ ), while in  $([\text{Au}(\text{NCH})_2][\text{AuCl}_4])_n$  models ( $n = 1, 2$ ), strong LMLCT and MLMLCT components were identified.

#### Disclosure statement

The authors declare that they have no known competing for financial interests or personal relationships that could have appeared to influence the work reported in this paper.

#### Funding

Financial support of this work under Fondecyt project 1180158 is gratefully appreciated.

#### References

- [1] Pyykkö P. Strong closed-shell interactions in inorganic chemistry. *Chem Rev.* 1997;97:597–636.
- [2] Pyykkö P, Runeberg N, Mendizabal F. Theory of the  $d^{10}$ - $d^{10}$  closed-shell attraction: I. Dimers near equilibrium. *Chem Eur J.* 1997;3:1451–1457.
- [3] Runeberg N, Schütz M, Werner H-J. The aurophilic attraction as interpreted by local correlation methods. *J Chem Phys.* 1999;110:7210–7215.
- [4] Pyykkö P. Theoretical chemistry of gold. *Angew Chem Int Ed.* 2004;43:4412–4456.
- [5] ÓGrady E; Kaltsoyannis N. Does metallophilicity increase or decrease down group 11? Computational investigations of  $[\text{Cl-M-PH}_3]_2$  ( $M = \text{Cu, Ag, Au, [111]}$ ). *Phys Chem Chem Phys.* 2004;6:680–687.
- [6] Dolg M, Pyykkö P, Runeberg N. Calculated structure and optical properties of  $\text{Tl}_2\text{Pt}(\text{CN})_4$ . *Inorg Chem.* 1996;35:7450–7451.
- [7] Pyykkö P. Theoretical chemistry of gold II. *Inorg Chim Acta.* 2005;358:4113–4130.
- [8] Schmidbaur H. In gold-Progress in chemistry, Biochemistry and Technology. New York: John Wiley & Sons; 1999.
- [9] Gimeno MC, Laguna A. In: McCleverty C, Meyer TJ, editors. *Comprehensive coordination chemistry 1*, Vol. 6. Amsterdam: Elsevier; 2004. pp. 911–1145.
- [10] Schmidbaur H, Schier A. A briefing on aurophilicity. *Chem Soc Rev.* 2008;37:1931–1951.
- [11] Schmidbaur H, Schier A. Aurophilic interactions as a subject of current research: an up-date. *Chem Soc Rev.* 2012;41:370–412.
- [12] Fackler JP. Copper, gold and nickel clusters with and without metal–metal bonds in 50 years of Fackler group chemistry. *Inorg Chim Acta.* 2015;424:83–90.
- [13] Tárkányi G, Király P, Pálkás G, et al. Conformational analysis of a helically distorted gold(I) macrocycle derived from xantphos: evidence for the aurophilic Au–Au interaction from NMR. *Magn Reson Chem.* 2007;45:917–924.
- [14] Deák A, Megyes T, Tárkányi G, et al. Synthesis and solution- and solid-state characterization of gold(I) rings with short Au...Au interactions. Spontaneous resolution of a gold(I) complex. *J Am Chem Soc.* 2006;128:12668–12670.
- [15] Wong KM-C, Au VK-M, Yam VW-W. In: Reedijk J, Poeppelemer K, editors. *Comprehensive inorganic chemistry II*. 2nd ed. Oxford, UK: Elsevier; 2013. pp. 59–130.
- [16] Yam VW-W, Au VK-M, Leung SY-L. Light-Emitting self-assembled materials based on  $d^8$  and  $d^{10}$  transition metal complexes. *Chem Rev.* 2015;115:7589–7728.
- [17] López-de-Luzuriaga JM, Monge M, Olmos ME. Luminescent aryl-group eleven metal complexes. *Dalton Trans.* 2017;46:2046–2067.
- [18] Donamaria R, Gimeno MC, Lippolis V, et al. Tuning the luminescent properties of a Ag/Au tetranuclear complex featuring metallophilic interactions via solvent-dependent structural isomerization. *Inorg Chem.* 2016;55:11299–11310.
- [19] Liptrott DJ, Power PP. London dispersion forces in sterically crowded inorganic and organometallic molecules. *Nature Reviews Chemistry.* 2017;1. doi:10.1038/s41570-016-0004.
- [20] Mendizabal F, Reyes D, Olea-Azar C. Complexes self-associate by hydrogen bonding and metallophilic attraction: theoretical study. *Int J Quantum Chem.* 2006;106:906–912.
- [21] Magnko L, Schweizer M, Rauhut G, et al. A comparison of metallophilic attraction in  $(\text{X-M-PH}_3)_2$  ( $M = \text{Cu, Ag, Au; X = H, Cl}$ ). *Phys Chem Chem Phys.* 2002;4:1006–1013.
- [22] Pyykkö P. Theoretical chemistry of gold. III. *Chem Soc Rev.* 2008;37:1967–1997.
- [23] Fernando A, Weerawardene KLD, Karimova NV, et al. Quantum mechanical studies of large metal, metal oxide, and metal chalcogenide nanoparticles and clusters. *Chem Rev.* 2015;115:6112–6216.
- [24] Reimers JR, Ford MJ, Marcuccio SM, et al. Competition of van der Waals and chemical forces on gold–sulfur surfaces and nanoparticles. *Nature Reviews Chemistry.* 2017;1. doi:10.1038/s41570-0017.
- [25] Chi Y, Chou PT. Transition-metal phosphors with cyclometalating ligands: fundamentals and applications. *Chem Soc Rev.* 2010;39:638–655.
- [26] Lin WP, Liu S-J, Gong T, et al. Polymer-Based resistive memory materials and devices. *Adv Mater.* 2014;26:570–606.

- [27] Blake AJ, Donamaria R, Lippolis V, et al. Unequivocal experimental evidence of the relationship between emission energies and aurophilic interactions. *Inorg Chem.* **2019**;58:4954–4961.
- [28] Lopez-de-Luzuriaga JM, Monge M, Olmos ME, et al. Stimuli-responsive solvatochromic Au(I)-Ag(I) clusters: reactivity and photophysical properties induced by the nature of the solvent. *Inorg Chem.* **2019**;58:1501–1512.
- [29] Yeung CLM, Yam VW-W. Luminescent cation sensors: from host-guest chemistry, supramolecular chemistry to reaction-based mechanisms. *Chem Soc Rev.* **2015**;44:4192–4202.
- [30] Zheng S-L, Nygren CL, Messerschmidt M, et al. Ligand-unsupported Au(I) chains with short Au(I)⋯Au(I) contacts. *Chem Commun.* **2006**;42:3711–3713.
- [31] Böge M, Heck J. Molecular gold wire from mixed-valent Au<sup>I/III</sup> complexes. *Chem Eur J.* **2016**;22:6787–6792.
- [32] Perdew J, Burke K, Ernzerhof M. Generalized gradient approximation made simple. *Phys Rev Lett.* **1996**;77:3865–3868.
- [33] Becke AD. Density-functional exchange-energy approximation with correct asymptotic behavior. *Phys Rev A.* **1988**;38:3098–3100.
- [34] Becke AD. Perspective: Fifty years of density-functional theory in chemical physics. *J Chem Phys.* **2014**;140:18A301–18.
- [35] Ehrlich S, Moellmann J, Reckien W, et al. System-Dependent dispersion coefficients for the DFT-D3 treatment of adsorption processes on ionic surfaces. *Chem Phys Chem.* **2011**;12:3414–3420.
- [36] Habza P, Zahradnik R. Intermolecular interactions between medium-sized systems. Nonempirical and empirical calculations of interaction energies. Successes and failures. *Chem Rev.* **1988**;88:871–897.
- [37] Bauernschmitt R, Ahlrichs R. Treatment of electronic excitations within the adiabatic approximation of time dependent density functional theory. *Chem Phys Lett.* **1996**;256:454–464.
- [38] Winter NO, Hättig C. Scaled opposite-spin CC2 for ground and excited states with fourth order scaling computational costs. *J Chem Phys.* **2011**;134:184101–184115.
- [39] Gerenkamp M, Grimme S. Spin-component scaled second-order möller-plesset perturbation theory for the calculation of molecular geometries and harmonic vibrational frequencies. *Chem Phys Lett.* **2004**;392:229–235.
- [40] Turbomole: Ahlrichs R, Bär M, Häser M, et al. Electronic structure calculations on workstation computers: the program system turbomole. *Chem Phys Lett.* **1989**;162:165–169.
- [41] Gaussian09: Frisch MJ, et al., Pittsburgh (PA), **2003**.
- [42] Andrae D, Häusserman M, Dolg H, et al. Energy-adjusted *ab initio* pseudopotentials for the second and third row transition elements. *Theor Chim Acta.* **1990**;77:123–141.
- [43] Bergner A, Dolg M, Küchle MW, et al. *Ab initio* energy-adjusted pseudopotentials for elements of groups 13–17. *Mol Phys.* **1993**;80:1431–1441.
- [44] Dunning T; Hay P. In: Schaefer H, editor. *Modern theoretical chemistry*, Vol. 3. New York: Plenum Press; **1997**. pp. 1–28.
- [45] Barrientos L, Miranda-Rojas S, Mendizabal F. Noncovalent interactions in inorganic supramolecular chemistry based in heavy metals. Quantum chemistry point of view. *Int J Quantum Chem.* **2019**;119:e25675.
- [46] Mendizabal F, Pyykkö P. Aurophilic attraction in binuclear complexes with Au(I) and Au(III). A theoretical study. *Phys Chem Chem Phys.* **2004**;6:900–905.
- [47] Carpenter JE, Weinhold F. Analysis of the geometry of the hydroxymethyl radical by the “different hybrids for different spins” natural bond orbital procedure. *J Mol Struct.* **1988**;169:41–62.
- [48] Roundhill DM, Fackler JP. In *Optoelectronic properties of inorganic compounds*. New York: Plenum Press; **1999**; p. 254.
- [49] Rawashdeh-Omary MA, Omary MA, Patterson HH. Oligomerization of Au(CN)<sub>2</sub><sup>-</sup> and Ag(CN)<sub>2</sub><sup>-</sup> ions in solution via ground-state aurophilic and argentophilic bonding. *J Am Chem Soc.* **2000**;122:10371–10380.